Coupling Fluid Flow to Hydrogel Fluidic Devices with Reversible "Pop-it" Connections

Journal:	*Lab on a Chip*
Manuscript ID	LC-ART-02-2021-000135
Article Type:	Paper
Date Submitted by the Author:	21-Feb-2021
Complete List of Authors:	Abbasi, Reha; Montana State University, Chemical & Biological Engineering; Montana State University LeFevre, Thomas; Montana State University, Chemical & Biological Engineering Benjamin, Aaron; Montana State University Bozeman, Mechanical and Industrial Engineering Department Thornton, Isaak; Montana State University, Mechanical and Industrial Engineering Department Wilking, James; Montana State University, Chemical & Biological Engineering

SCHOLARONE™
Manuscripts

Coupling Fluid Flow to Hydrogel Fluidic Devices with Reversible "Pop-it" Connections

Reha Abbasi[1,2], Thomas B. LeFevre[1,2], Aaron D. Benjamin[1,3], Isaak J. Thornton[1,3] and James N. Wilking[1,2]*

[1]Center for Biofilm Engineering,

[2]Chemical and Biological Engineering Department, and

[3]Mechanical and Industrial Engineering Department,

Montana State University, 214 Roberts Hall,

Bozeman, MT, 59717, USA

[*]Address correspondence to james.wilking@montana.edu

ABSTRACT

Hydrogels are soft, water-based polymer gels that are increasingly used to fabricate free-standing fluidic devices for tissue and biological engineering applications. In many of these applications, pressurized liquid must be driven through the hydrogel device. To couple pressurized liquid to a hydrogel device, a common approach is to insert tubing into a hole in the gel; however, this usually results in leakage and expulsion of the tubing, and other options for coupling pressurized liquid to hydrogels remain limited. Here, we describe a simple coupling approach where microfluidic tubing is inserted into a plastic, 3D-printed bulb-shaped connector, which "pops" into a 3D-printed socket in the gel. By systematically varying the dimensions of the connector relative to those of the socket entrance, we find an optimal head-socket ratio that provides maximum resistance to leakage and expulsion. The resulting connection can withstand liquid pressures on the order of several kilopascals, three orders of magnitude greater than traditional, connector-free approaches. We also show that two-sided connectors can be used to link multiple hydrogels to one another to build complex, reconfigurable hydrogel systems from modular components. We demonstrate the potential usefulness of these connectors by established long-term nutrient flow through a 3D-printed hydrogel device containing bacteria. The simple coupling approach outlined here will enable a variety of applications in hydrogel fluidics.

35

INTRODUCTION

Hydrogels are soft, water-based polymer gels[1-4] with widespread applications in medicine[5, 6] and bioengineering.[7, 8] While hydrogels have long been incorporated into fluidic devices[9, 10], the development of stand-alone hydrogel fluidic devices and other hydrogel fluidic elements with complex three-dimensional structures has historically been limited. However, recent advances in rapid fabrication are now enabling the creation of hydrogel-based fluidic elements and free-standing devices with complex, high-resolution structures.[11-14] For example, hydrogel-based photoreactors,[15] bioreactors,[16] and a variety of engineered tissues with intricate structures[17-20] and microscale vasculature[11, 15, 16, 20-24] have been created. As rapid fabrication technologies continue to advance, the use of hydrogel-based fluidic devices are expected to expand.[25]

To drive liquid through a fluidic device, tubing containing liquid must be coupled to the device. For devices composed of hydrogel, this presents a challenge.[25] A common solution, used in soft polydimethylsiloxane (PDMS)-based microfluidics, is to simply insert microfluidic tubing into a hole in the device.[26, 27] In a PDMS device, static friction between the tubing and PDMS prevents the tubing from slipping out of the device and allows the formation of a robust, high-pressure seal.[28] However, when this approach is attempted with hydrogel devices, a thin layer of water on the surface of the gel lubricates the interaction between the gel and tubing and allows the tubing to slip out under relatively low pressure. Adhesives and barb-type connectors have been shown to provide stable, high-pressure seals,[29] but simple, reversible connector solutions are still needed, and the lack of such technologies limits the development of hydrogel-based fluidics.

Here, we describe a simple, reversible, plug-based connector designed to couple microfluidic tubing to a hydrogel-based fluidic device, to allow for pressurized liquid flow through the system. The connection consists of a 3D-printed plastic plug inserted into a matching spherical socket in a 3D-printed hydrogel, which is then held in place by the elasticity of the gel. We call this a "pop-it" connector. The connection can easily be removed and reinserted, allows for rotation around the long axis of the connector, and can also be used to link individual hydrogel modules to one another to build complex, reconfigurable fluidic hydrogel systems. To characterize the connection, we systematically vary the diameter of the connector head relative to the diameter of the gel socket entrance, measure both the force required for insertion and the liquid pressure the resulting seal

65   can withstand, and find the head-socket ratio that provides the maximum resistance to leakage and

66   expulsion. To demonstrate the usefulness of these connectors, we use them to deliver nutrient broth

67   to a 3D printed hydrogel containing bacteria for over a day. The simple and robust connector

68   design should enable a variety of hydrogel fluidic applications.

69   **RESULTS & DISCUSSION**

70   To illustrate the standard approach for driving liquid into soft microfluidic devices, we create a

71   cylindrical, mm-scale hole in a PDMS-based microfluidic device using a biopsy punch and insert

72   plastic tubing into the hole (**Fig. 1a**). The outer diameter of the tubing (OD = 1.09 mm) is larger

73   than the inner diameter of the hole (ID = 1.05 mm) and is held in place by static friction. This

74   friction is enough to withstand the pressure needed to drive liquids through the device, which can

75   approach $\Delta P \approx 10^3$ Pa.[30, 31]

76   By contrast, when tubing is inserted into a hydrogel fluidic device, friction between the tubing and

77   gel is insufficient to resist even very small pressures. To demonstrate this, we 3D print a cm-scale

78   polyethylene glycol diacrylate (PEG-DA) hydrogel (10 w/w%) containing a single straight channel

79   of length, l = 12 mm and diameter, D = 0.8 mm and insert microfluidic tubing into the channel.

80   The outer diameter of the tubing (OD = 1.32 mm) is larger than the inner diameter of the channel

81   entrance (ID = 1.20 mm) corresponding to a gel strain of $\gamma \approx 0.1$, so the gel exerts a radial

82   compressive stress on the tubing (**Fig. 1b**). When we drive water through the hydrogel using a

83   syringe pump at a low flow rate (Q = 200 μL/min), we observe that the seal begins to leak in less

84   than 10 seconds, and the tubing, with an inserted section length, $l \approx 3$ mm, is forced out of the

85   hydrogel in less than 100 seconds. This is illustrated by the series of time-resolved images in **Fig.**

86   **1b**. While the failure rate depends on a variety of factors such as gel elasticity, surface moisture,

87   surface roughness, and gel strain, leakage and tubing expulsion from hydrogel-based fluidic

88   devices occurs consistently and at low flow rates. Failure occurs even more frequently when

89   hydrogels with smaller channels and more complex vasculature are used due to the higher

90   pressures required to drive flow.

91   To address this issue, we design and fabricate a plastic connector and gel socket pair that serves to

92   secure fluidic tubing to the hydrogel. Our connector is plug-shaped, and 3D printed using a

93   photopolymerizable plastic (see Methods). Microfluidic tubing is inserted into the connector and

94   the two are held together with static friction (**Fig. 2a**). To couple the tubing and connector assembly

95   to a hydrogel, a matching socket is printed at the channel inlet to the hydrogel, and the connector

96   is inserted into the socket, as shown in **Fig. 2b-c**. The design is such that a lip of gel at the channel

97   orifice is stretched during connector insertion and relaxes to form a tight seal around the connector

98   after insertion. We call this a "pop-it" connection. These connectors are simple and easy to

99   manufacture. For example, the batch of connectors shown in **Fig. 2d** ($n \approx 100$) can be fabricated

100   in less than two hours. A hydrogel with pop-it connectors inserted on both inlet and outlet ports is

101   shown in the photograph in **Fig. 2e**.

102   Provided a connector is matched with a smaller-diameter, appropriately sized gel socket, the gel

103   will form a seal and the elasticity of the gel will resist removal. Appropriate sizing is based on the

104   condition that the head of the connector, with diameter D_c, is larger than the inner neck diameter

105   D_g of the gel socket ($D_c/D_g \geq 1$; Fig. 2b, c). Intuitively, we expect the seal to improve as D_c/D_g

106   increases; however, if D_c/D_g is too large, the gel will fracture during connector insertion. To

107   determine the magnitude of the forces associated with connector insertion as well as the largest

108   achievable D_c/D_g ratio without gel fracture, we systematically vary D_c/D_g and for each condition

109   measure the force required for insertion as well as the maximum liquid pressure the seal can

110   withstand. For these measurements, we fix the gel neck entrance size (D_g = 2.30 mm) and

111   systematically vary the connector head size (2.70 mm $\leq D_c \leq$ 3.50 mm). In this way, we vary the

112   D_c/D_g ratio from 1.17 to 1.52.

113   To measure the force required for connector insertion as a function of D_c/D_g, we use the normal

114   force sensor of a mechanical rheometer (**Fig. 3a**). For each measurement, a connector with a

115   defined D_c is mounted on the upper rheometer plate and brought down towards the gel at a fixed

116   velocity (v = 10 μm/s). Before the connector and gel come into contact, the normal force F is zero.

117   When the two contact, the normal force jumps, and increases as the connector is forced into the

118   gel socket, deforming the gel. The normal force increases to a maximum, F_{max} and then drops back

119   to a value close to zero as the connector locks into the gel socket. A representative measurement

120   is shown in **Fig. 3b**. For each D_c, we measure multiple force-displacement curves (n = 3-7) and

121   co-plot these data. We observe that F_{max} increases with increasing D_c (**Fig. 3c**). For connectors

122   with $D_c > 3.60$ we observe that the gel fractures when the connector is inserted (data not shown).

123   This sets an upper limit for D_c/D_g for this connector geometry and gel formulation.

4

124   To understand the forces resisting connector insertion, we convert the measured force to a stress τ

125   by dividing the averaged F_{max} for each D_c by the maximum contact area between the connector

126   and gel (see Methods and ESI). We then define the maximum gel strain during connector insertion

127   to be $\gamma \approx (D_c - D_g)/D_g$, and plot τ as a function of γ (**Fig. 3d**). We find that the data is fit well by a

128   straight line, even for large $\gamma > 0.5$. This is consistent with elastic behavior, where $\tau = G_e\gamma$ and G_e

129   is the elastic modulus of the gel.[32] From our fit, we find the elastic modulus to be $G_e = 11.6 \pm 1.1$

130   kPa. To compare this result from insertion force measurements with bulk measurements, we

131   perform shear rheometry on large hydrogels and find the elastic modulus of the gel to be $G_e = 10.7$

132   ± 0.2 kPa (**Fig. 3e**). This confirms that the gel is deformed elastically for this D_c/D_g range and that

133   the elasticity of the gel resists connector insertion. Here, because there were no device design

134   constraints, the overall dimensions of the hydrogel fluidic device were sized such that the printed

135   socket did not interfere with the macroscale structure or functionality of the gel; however, socket

136   size may become an issue for very small devices. For example, practical considerations like

137   physical handling and insertion of the connector into the socket will limit the smallest connector

138   and socket that can be used. For small socket sizes, the gel lip thickness may also become so thin

139   that it is unable to withstand deformation without gel fracture. Also, in situations where important

140   structural features of the gel device are in close proximity to the socket, gel deformation induced

141   by connector insertion may impact these features.

142   Next, we test the maximum liquid pressure, P_{max} that the pop-it connections can withstand before

143   connector leakage and expulsion. To apply a well-defined hydrostatic pressure, we attach the pop-

144   it connector to a reservoir of water that can be raised and lowered in a controlled manner (see

145   Methods and ESI). To apply static pressure without needing to account for pressure loss due to

146   liquid flow, we use hydrogel sockets with a closed inner surface that are not connected to open

147   channels in the gel. For each experiment, we systematically increase the hydrostatic pressure, P in

148   increments ranging from 0.025 Pa to 10 Pa until connection failure is observed. We do this over

149   the range: $1.16 \leq D_c/D_g \leq 1.67$ by fixing the socket size ($D_g = 2.15$ mm) and systematically varying

150   D_c. For each connector ratio, we measure P_{max} multiple times ($n \approx 12$) by performing up to 3 repeat

151   measurements on 4 to 5 different hydrogels. Hydrogels are elastically deformed during insertion

152   and removal, and we observe no statistically significant trend in P_{max} with repeated measurements

153   on the same gel. While the gel formulation used in these experiments has a swelling ratio less than

154   1% in distilled water[33], we equilibrate the gels for 24 h in distilled water to mitigate any swelling

155   effects.

156   We find that P_{max} increases with γ, approaching values as high as $P_{max} \approx 3$ kPa (**Fig. 4**). These

157   pressures are three orders of magnitude greater than those we measure for connector-free couplings

158   ($P_{max} \approx 2.5 \pm 1.5$ Pa, $n = 3$ hydrogels) and are equivalent to pressures generated in PDMS-based

159   microfluidic devices. Pressure of this magnitude could be used to generate significant flow rates

160   in large channels ($Q \approx 170$ mL/min, cylindrical channel with $D = 0.8$ mm and $l = 12$ mm, see

161   Methods) and are large enough to drive flows through highly vascularized tissues.[34] Interestingly,

162   though both connector insertion and expulsion require gel deformation, P_{max} increases

163   exponentially with γ, while [F_{max}/A] increases linearly with γ (Fig. 3c). This may be because for

164   large D_c the connector head becomes asymmetric along the axis of the cylinder (see images in

165   ESI); thus, the contact area between the connector and gel during insertion and removal may be

166   quite different. In addition, the gel socket lip is asymmetric and may deform differently during

167   insertion and removal. This apparent hysteresis is supported by preliminary normal force

168   measurements of connector insertion and removal (see ESI). While understanding this hysteresis

169   is outside the scope of this paper, this warrants further investigation. Here, the liquids we flow

170   through the gel are the same as the liquids used to equilibrate the gel; if liquids with different

171   compositions and osmolalities are used, potential swelling or shrinkage may impact P_{max}.

172   Pop-it connectors can also be used to connect modular gels to one another. For example, two-

173   sided, dumbbell-shaped connectors (**Fig. 5a**) matched to 3D printed sockets in opposing gels can

174   be used to bring adjacent gel cubes into contact and hold them in place. For example, joining of

175   two hydrogel cubes using a two-sided connector is shown in a series of images in **Fig. 5b, c**. To

176   further demonstrate this modularity, we print four hydrogel cubes (edge length, $l_c = 9$ mm), three

177   of which contain a straight cylindrical channel ($D = 1.20$ mm) running from one cube face to the

178   opposing face, and one cube with three cylindrical channels running from three different cube

179   faces and joining at a single intersection point. We dye these cubes with food coloring to highlight

180   their individuality, connect them using two-sided pop-it connectors, and drive water through the

181   assembly with one-sided pop-it connectors coupled to microfluidic tubing. Images of the gel

182   modules and the assembly are shown in **Fig. 5d, e**. The connectors form an excellent seal between

183   hydrogels, allowing for liquid flow. This approach could be used to build complex, reconfigurable

184   hydrogel systems from simple modular components. We note that a variety of connector types
185   exist for connecting modular microfluidic components to one another[35, 36] including self-aligning
186   magnetic interconnects[37] and integrated microfabricated gaskets[38]; however, these technologies
187   have not been demonstrated for use with hydrogels.

188   Pop-it connections offer additional advantages. First, pop-it connections allow for rotation around
189   the long axis of the connector. To demonstrate this, we attach two hydrogels together with a two-
190   sided connector and rotate the upper (blue) hydrogel by 45° around the z-axis without disturbing
191   the connection (**Fig. 6a-c**). This rotational degree of freedom could be used for reconfigurable
192   modular assemblies for structure-function studies and soft robotics. Second, two-sided connectors
193   can be used to bring two hydrogel modules into contact together to allow for molecular diffusion
194   from one module to another. To demonstrate this, we bring two hydrogel cubes together with a
195   dumbbell shaped connector and observe the diffusion of red dye from one cube into the other (**Fig.**
196   **6d-f**). This could be used to establish well-defined concentration gradients in engineered tissues.
197   Third, the reversibility of the pop-it connection allows one to change the composition of the liquid
198   driven through a given hydrogel during an experiment. To demonstrate this, we introduce one
199   colored oil to a hydrogel module, followed by a second colored oil from a separate tubing source
200   (**Fig. 6g, h**). This approach could be used to alter the media conditions supplied to living cells
201   embedded in hydrogel. This rapid exchange is not feasible for connections requiring adhesive.[29]

202   Finally, to demonstrate a clear application of the pop-it connection, we 3D-print a hydrogel cube
203   containing *Pseudomonas aeruginosa* (pMF230; constitutively expressing GFP) with a single
204   straight channel with connection sockets at both ends of the channel and use pop-it connections on
205   either end to establish nutrient flow through the hydrogel. We use a plastic 3D-printed holder to
206   stabilize the gel, connectors, and tubing (**Fig. 6i**). We store the entire assembly in an incubator at
207   37 °C and 100% relative humidity and drive tryptic soy broth (TSB) media at a flow rate of 2 mL/h
208   through the gel. After 24 h, we cross-section the hydrogel and image the GFP intensity with
209   confocal microscopy. A duplicate bacteria-laden hydrogel is cross-sectioned at $t = 0$ and imaged
210   as well for comparison. The images in **Fig. 6j, k** show clear microbial growth in the hydrogel
211   supplied with media.

212   The connector design presented here could be modified in a variety of ways. For example, the
213   shape of the connector and socket could be optimized for ease of insertion, for improved seal

214   formation, or to better distribute stress in the hydrogel. Here, we use a bulb-shaped connector, but

215   other connector geometries such as screw shapes and configurations with different rotational and

216   axial symmetry could be explored. In addition, fabrication methods other than 3D printing could

217   be used to structure the connector socket in the hydrogel. For example, a casting approach like that

218   used in soft lithography-based could be used, [39-41] and, the creation of overhanging features in the

219   negative mold could be achieved using two-photon polymerization techniques.[42, 43] Pop-it

220   connectors could also be integrated into hybrid hydrogel/PDMS systems.[10] Finally, a wide variety

221   of hydrogel formulations could be explored to improve or optimize connector performance.[44] Gel

222   mechanical properties could be varied by controlling monomer and crosslinker chemistries [45],

223   molecular weight[46], gel concentration,[46] and by the addition of filler materials.[47] In addition,

224   alginate,[48] agarose,[48] gelatin methacryloyl (GelMA),[49] poly(vinyl alcohol) (PVA),[50] and double-

225   network hydrogels with enhanced strength and elasticity[47] could be explored.

226   **CONCLUSIONS**

227   In conclusion, the 3D printed "pop-it" connection presented here represents the first reported

228   hydrogel connection mechanism for coupling tubing to hydrogel fluidic devices in a stable,

229   reversible manner to allow for liquid flow. Pop-it connectors mount into well-defined 3D printed

230   sockets by simple insertion and are held in place by the elasticity of the hydrogel, rather than static

231   friction. Using this connection, we show that it is possible to drive fluid flow while sustaining

232   pressures up to $\Delta P \approx 3$ kPa, which is three orders of magnitude greater than the standard connector-

233   free approach and equivalent to the pressures required to drive flow through standard PDMS-based

234   microfluidic devices. We demonstrate that a two-sided connector can be used to couple two

235   hydrogels together to construct modular assemblies with intermodular diffusion. Lastly, we

236   demonstrate that pop-it connectors can be used to establish long-term nutrient flow to hydrogels

237   to sustain the growth and viability of bacteria in the gel. These pop-it connectors will enable a

238   variety of hydrogel applications by allowing for reliable, leak-free flow.

239

240   **METHODS**

241   *Hydrogel 3D Printing.* Hydrogels were designed using CAD software (Autodesk, Fusion 360) and

242   3D printed using a commercial stereolithography 3D printer (Formlabs, Form 1+). For the aqueous

243   resin formulation, poly(ethylene glycol) diacrylate (PEG-DA) was used as a monomer (10 wt%,

244   Sigma-Aldrich, M_n 700), lithium phenyl-2,4,6-trimethylbenzoylphosphinate (LAP) was used as a

245   photoinitiator (0.1 wt%, Tokyo Chemical Industry), and tartrazine was used as a photoblocker

246   (0.075 wt%, Alfa Aesar). Prepared resin solutions were poured into the printer resin tray. To

247   fabricate gels with well-defined and open structures, resin formulation and light exposure

248   conditions were selected for optimal printing.[11] To ensure adhesion of hydrogel to the print head,

249   microscopy slides (Fisherbrand Colorfrost, 25 mm × 75 mm × 1 mm) were pretreated with Bind-

250   Silane (2.0 vol%, GE Healthcare, 17-1330-01). Microscopy slides were submerged in the Bind-

251   Silane solution for five minutes then baked at 100 °C for another five minutes. Treated slides were

252   attached to the custom-made print head with a UV bonding adhesive (Norland Products).[51]

253   Hydrogel CAD files are available in ESI. The printing process proceeds by photopolymerizing the

254   object layer-by-layer as described elsewhere.[52]

255   ***Connector 3D Printing.*** Connectors were designed using CAD software (Autodesk, Fusion 360)

256   and 3D printed with a commercial stereolithography 3D printer (Formlabs, Form 3) using a

257   methacrylic acid ester-based resin (Formlabs, Clear Resin). After printing, connectors were

258   washed with isopropyl alcohol and post-cured with a benchtop ultraviolet light. Formlabs resins

259   are resistant to ethanol and UV light, both of which can be used for sterilization. As an alternative,

260   Formlabs High-Temperature resin could be used to create autoclavable connectors. Connector

261   CAD files are available in ESI.

262   ***Liquid Flow.*** To drive water through a hydrogel, a plastic syringe (60 mL Soft-Ject Luer Lock,

263   Henke Sass Wolf) was filled with water and mounted into a syringe pump (World Precision

264   Instruments, Model AL-4000). A blunt, 20-gauge dispensing needle was attached to the syringe

265   end with a luer lock fitting and polyethylene tubing (Scientific Commodities Inc., I.D. = 0.86 mm;

266   O.D. = 1.32 mm). The other end of the tubing, with or without attached pop-it connector, was then

267   inserted into the 3D printed hydrogel. For the hydrogels in Fig. 1 and 2, oil-based red and yellow

268   paint diluted with silicone oil (AR20) was used to highlight the channels.

269   ***Hydrostatic Pressure Measurements***. To determine the pressure required for connector failure,

270   we constructed a custom experimental setup capable of applying well-defined hydrostatic

271   pressures (**SI Fig. 1**). The mechanized system consisted of a microcontroller (Elegoo UNO R3), a

272   stepper motor driver (TB6600), and two stepper motors with lead screws (NEMA 17 with 150 mm

273   T8 lead Screws). The lead screws provided controlled linear movement with a minimum step size

274   of 2.5 μm. A water reservoir was mounted to the stepper motor lead screws and connected to the

275   hydrogel through tubing and a pop-it connector. The reservoir was incrementally raised using the

276   stepper motors until the connection between the connector and the hydrogel failed. The height

277   differential between the top of the water reservoir and the pop-it connector was then used to

278   determine the maximum liquid pressure, P_{max} by calculating the hydrostatic pressure at that point

279   using $P_h = \rho g h$, where ρ is density of the fluid, g is gravitational force and h is the height of the

280   fluid. A video of a representative experiment is shown in **Video S1**. The data in Fig. 4 is fit to the

281   following function: $\Delta P = a e^{b\gamma}$ where $\gamma \approx (D_c - D_g)/ D_g$, $a = 0.056$, and $b = 5.48$.

282   ***Flow Rate Estimates.*** To estimate the flow rates that our pop-it connections are capable of

283   withstanding, we calculate the volumetric flow rate, Q through a cylindrical channel of diameter,

284    $D = 0.8$ mm and length $l = 12$ mm using the Hagen-Poiseuille equation.

285    $$Q = \frac{\Delta P \pi D^4}{128 \eta l}$$

286   Here, η is the dynamic viscosity of the liquid and $\Delta P = \Delta P_{max}$. For water and $\Delta P_{max} = 3$ kPa, we

287   find $Q = 170$ mL/min.

288   ***Rheometry and Force Measurements.*** A mechanical rheometer (TA Instruments AR-G2) was

289   used to perform two types of measurements: standard shear rheometry and non-standard normal

290   force measurements. Small amplitude shear rheometry measurements over a range of frequencies,

291    $\omega = 0.01$ Hz – 1 Hz and strain amplitudes, $\gamma = 0.001 – 0.05$ were performed after mounting coin-

292   shaped 3D-printed hydrogels (sample thickness, $h = 3$ mm; sample diameter, $D_s = 20$ mm) in a

293   parallel plate geometry (plate diameter, $D_p = 20$ mm). Normal force measurements were performed

294   by attaching individual connectors to the upper rheometer head with double-sided adhesive tape.

295   Then, a spot in the center of the lower rheometer plate was marked, 3D printed hydrogel samples

296   were mounted inside a 3D printed housing, and the housing placed on the lower plate in a well-

297   defined position. To further ensure axial alignment of the connector with the socket, the z-position

298   of the upper rheometer head was slowly lowered to approach the hydrogel allowing any necessary

299   adjustments to be made. To measure the normal force required to remove the connector from a

300   hydrogel socket, an inserted connector was retracted by lifting the upper rheometer plate away

301   from the gel. Each measurement took approximately 2-3 minutes in total; if the measurement was

302   prolonged, the hydrogel was kept hydrated by the addition of a small amount of water. The pressure

303   sensing unit of the rheometer is within the lower standing platform. Once the connector and gel

304   are in contact, the integrity of the connector adhesion to the upper geometry should not impact the

305   measurement. If this adhesion were to fail before contact, we would expect a sudden jump in the

306   force. Adhesion of the holder to the lower platform is less likely to fail, would result in a shift in

307   the xy-plane, and would easily be observed by visual inspection.

308

309   ***Measuring Contact Area of the Connector.*** The contact area, A used in Fig. 3d to calculate τ was

310   estimated using the "Measure" function in Fusion 360. For this, each connector CAD drawing was

311   used to estimate potential contact area of each connector on the inner walls of the hydrogel (See

312   supplementary). Estimating A is done by assuming that the hydrogel socket is stretching into the

313   shape of pop-it connector upon insertion. Also, since the surface area of the pop-it connector acting

314   on the hydrogel during F_{max} should not change for insertion and removal of the connector, the

315   same A values are valid to calculate pressure acting on the hydrogel during both insertion and

316   removal of the connector.

317

318   ***Growth of 3D Printed Bacteria.*** *Pseudomonas aeruginosa* (pMF230) is cultured overnight in

319   liquid TSB media with ampicillin (100 µg mL^{-1}). After 12+ h of growth, approximately 10^9

320   CFU/mL of planktonic bacteria is added to the bioink resin prior to the 3D printing. The pMF230

321   strain constitutively expresses GFP, so fluorescence intensity and colony size are used to measure

322   growth and viability. The hydrogel holder in Fig. 6i is 3D printed (Formlabs, Form 3, High

323   Temperature Resin) and autoclaved prior to assembly. After growth for 24 h at 37 C, the gel is

324   sectioned with a razor blade and imaged with a confocal microscope (Leica SP5; 5× air objective).

325

326   **Author Contributions:**

327   Conceptualization: A.D.B., R.A., and J.N.W.; Methodology: R.A., A.D.B., T.B.L., I.T., and

328   J.N.W; Investigation: R.A., A.D.B., T.B.L., and I.T.; Writing – Original Draft: R.A. and J.N.W.;

329   Writing – Review & Editing: R.A., A.D.B., T.B.L., I.T., and J.N.W; Funding Acquisition,

330   Resources, and Supervision: J.N.W.

331

332   **Conflicts of Interest:**

333   There are no conflicts to declare.
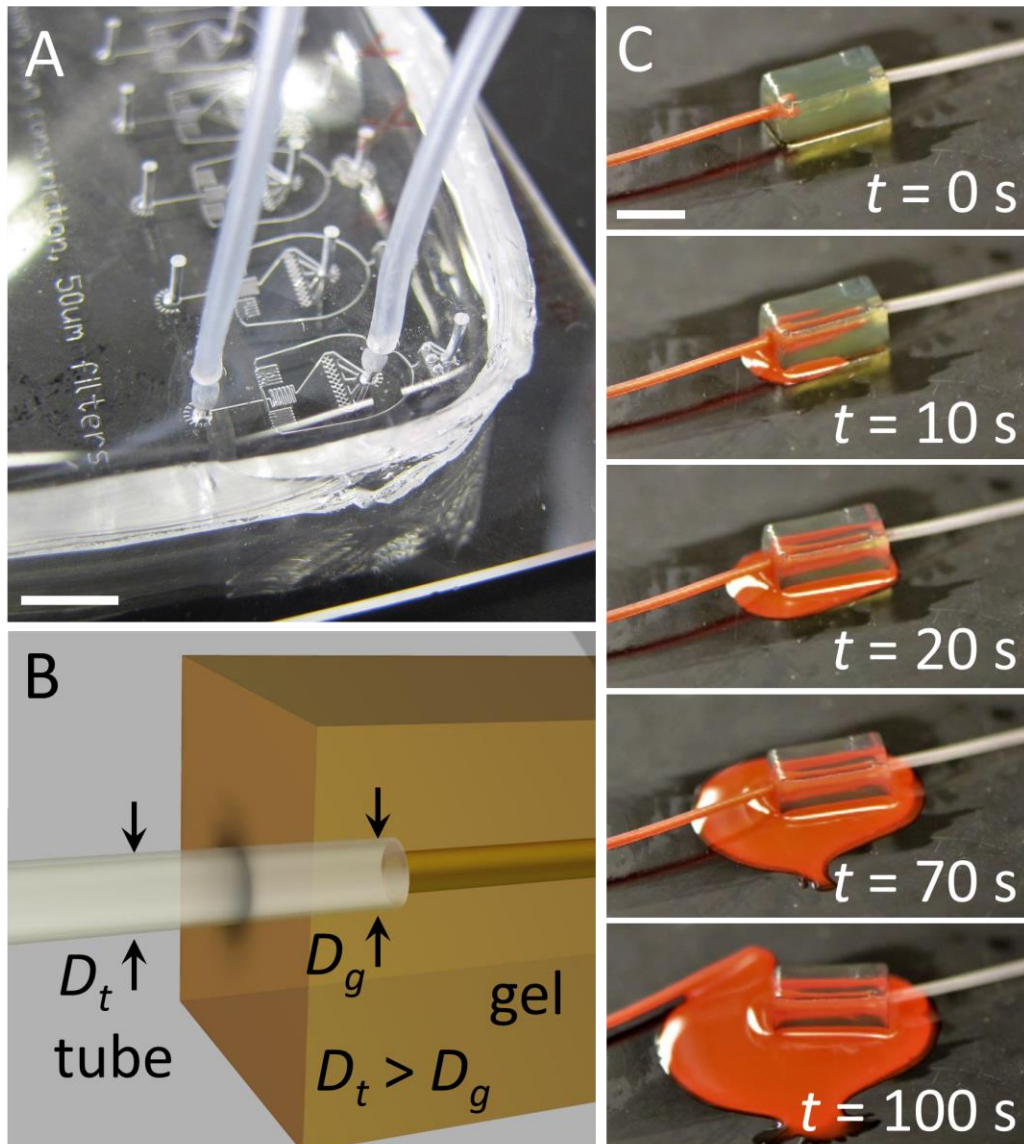
334

339

342

343

344

345

346

347

348

349

350

351
352   **Figure 1**: *Friction-based connections developed for traditional microfluidic devices fail when*
353   *applied to hydrogels.* (**A**) Liquid is introduced into a soft microfluidic device by punching a hole
354   in the PDMS and inserting larger diameter microfluidic tubing into the hole. Static friction prevents
355   the tubing from being expelled even for liquid pressures as high as $\Delta P \approx 10^3$ Pa. When the same
356   approach is applied to a 3D printed PEG-DA hydrogel, where (**B**) tubing is inserted into a smaller
357   diameter hole in the surface of the gel to a depth of 3 mm, (**C**) the tubing is expelled from the
358   hydrogel as liquid is forced into the gel at low pressure ($\Delta P \approx 1$ Pa). Scale bars in (A) and (C)
359   correspond to 5 mm and 10 mm, respectively.
360
361
362
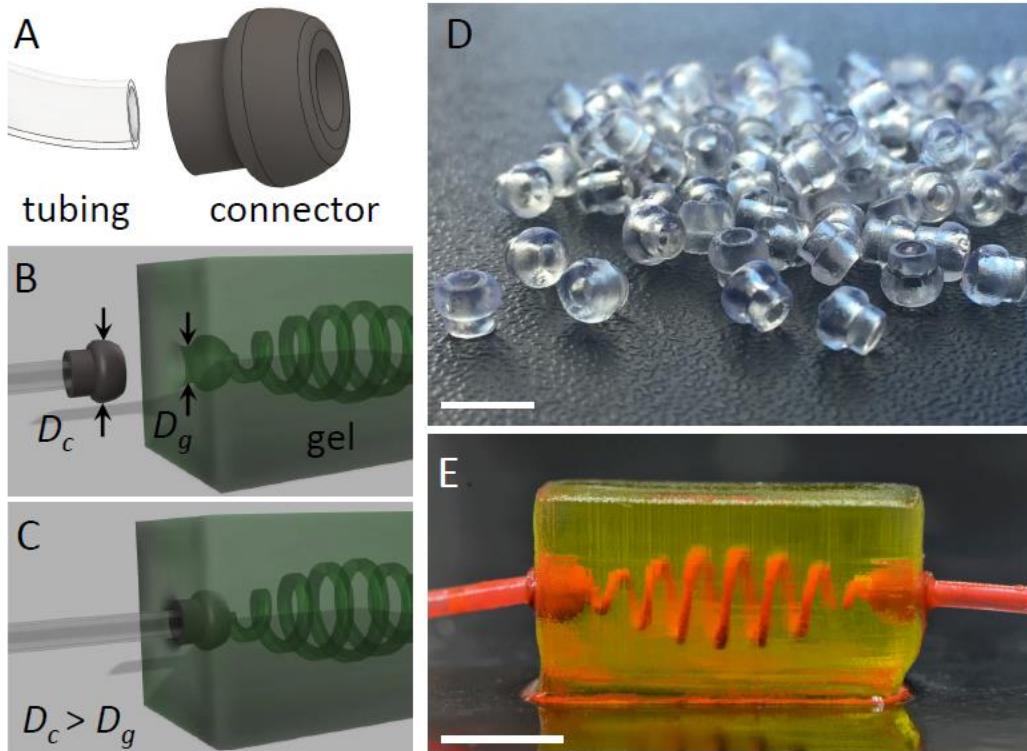
Figure 2: *Plastic 3D printed connector secures fluidic tubing to 3D printed hydrogel.* (**A**) CAD rendering of connector design. (**B, C**) Illustrations of connector insertion into 3D printed socket opening into a hydrogel channel. For a seal to form, the diameter of the connector head, D_c must be larger than the diameter of the gel socket neck, D_g. (**D**) Connectors can be rapidly printed and with high fidelity. (**E**) Connectors secure fluidic tubing to two ends of a 3D printed hydrogel. Channel is filled with an oil-based dye to highlight channel shape. Liquid beneath gel is not leaked oil, but residual water with color reflection from above. Scale bars in (D) and (E) correspond to 5 mm.
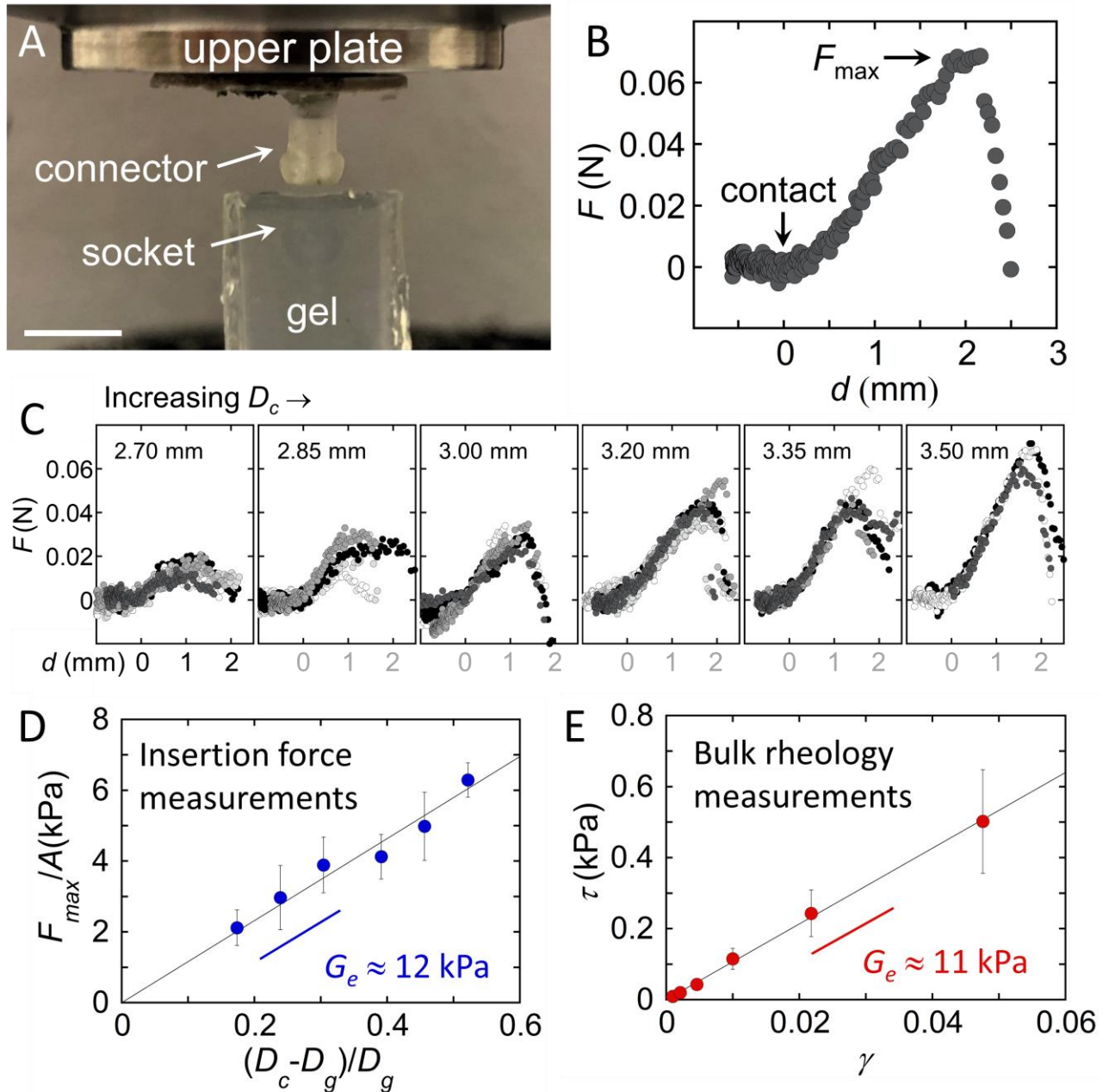
Figure 3: *Connector insertion into gel socket is governed by gel elasticity.* (**A**) Experimental setup for measuring the normal force resisting connector insertion into a gel socket. The upper plate of the rheometer brings the connector down into contact with the gel. The normal force, F is measured by a plate beneath the gel. Scale bar corresponds to 5 mm. (**B**) Representative plot of normal force F as a function of distance d for the experiment shown in (A) for D_c = 3.50 mm and D_g = 2.15 mm. (**C**) Force measurements for connectors of varying D_c and gels with fixed D_g = 2.15 mm. F_{max} increases with increasing D_c. Different colored symbols represent measurements on individual gels (n = 3-7 for each D_c). (**D**) Averaged F_{max} from (C) divided by the contact area A between the connector and gel provides a stress, which is plotted as a function of the maximum dimensionless strain: $(D_c - D_g)/D_g$. The slope of the curve provides the gel elastic modulus G_e. (**E**) Bulk rheology measurements on the gel provide a comparable value for G_e, confirming the role of gel elasticity.

15

389
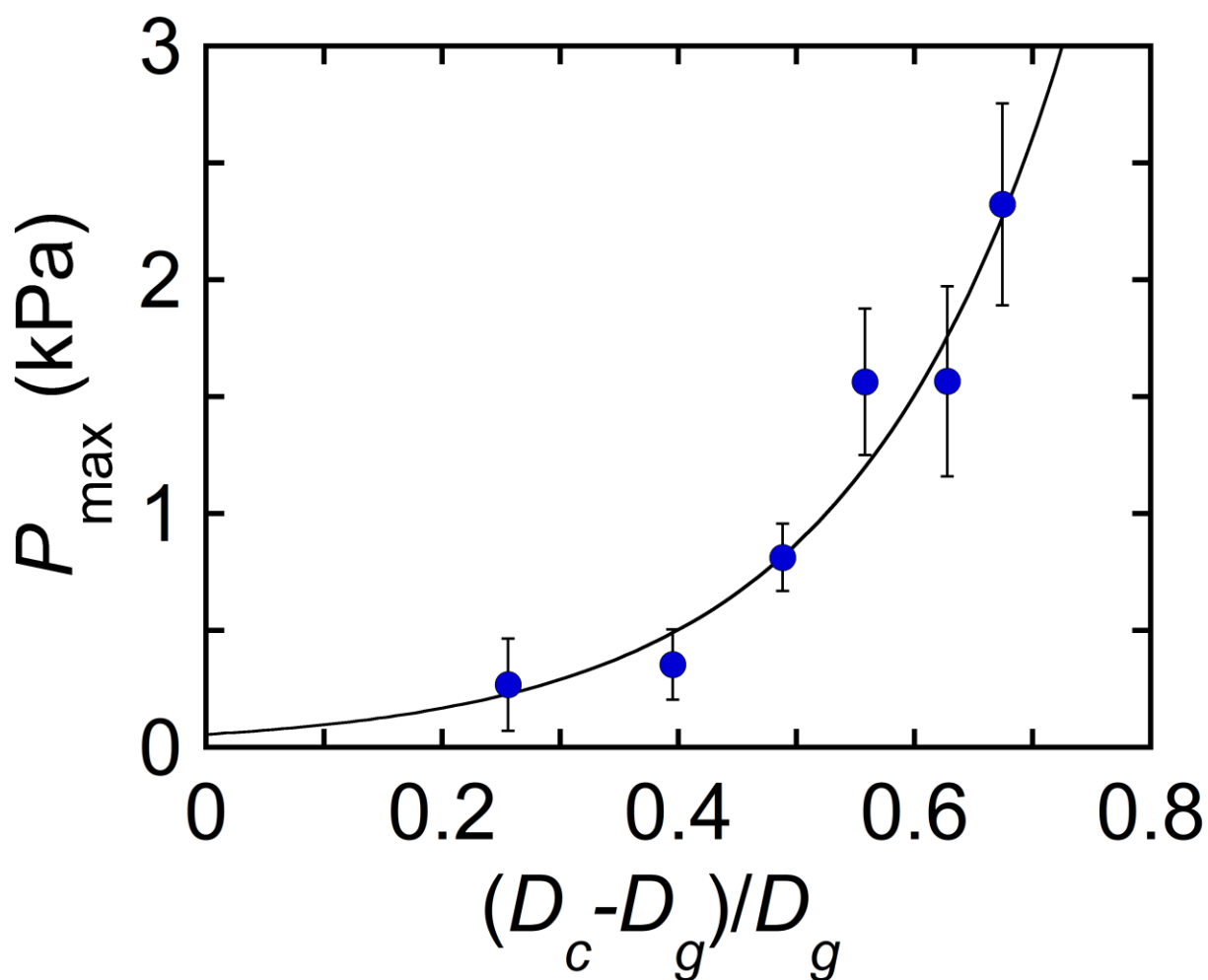
390
391
392   **Figure 4**: *Seal between connector and gel socket improves as the connector head diameter*
393   *increases relative to the gel neck diameter.* Maximum hydrostatic pressure at failure, P_{max}, plotted
394   as function of maximum gel neck strain during connector expulsion and fit to a simple exponential
395   increase (see Methods). For the connector with the largest head, the connection can withstand
396   pressures $\Delta P > 2.5$ kPa, three orders of magnitude greater than the pressures that standard,
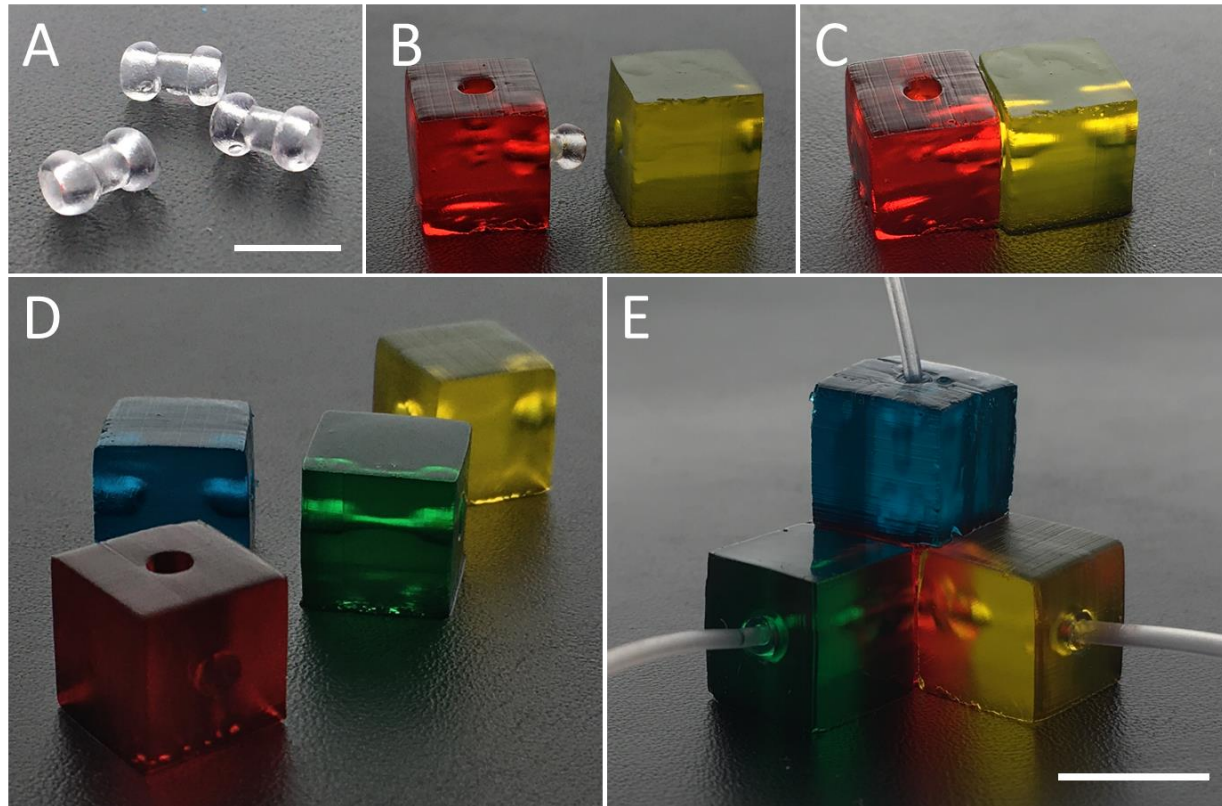397   connector free approaches can withstand ($\Delta P \approx 1$ Pa).

398
399
400
401
402
403
404

405

406

407 **Figure 5**: *Double-sided pop-it connectors can be used to build interconnected assemblies from*
408 *modular gels.* (**A**) Photograph of two-sided connectors. (**B, C**) Image series of two 3D printed
409 hydrogels joined using a two-sided connector. (**D, E**) Images of four 3D printed hydrogels joined
410 together using multiple two-sided connectors. Gels were colored with food dye before assembly
411 to illustrate modular nature of the assembly. The blue, green, and yellow cubes contain a single
412 straight channel running from one cube face to another. The red gel contains channels running
413 from three adjacent faces that connect in the center of the cube. The modular assembly does not
414 leak when water is driven through the assembly. Scale bars in (A) and (E) correspond to 5 mm and
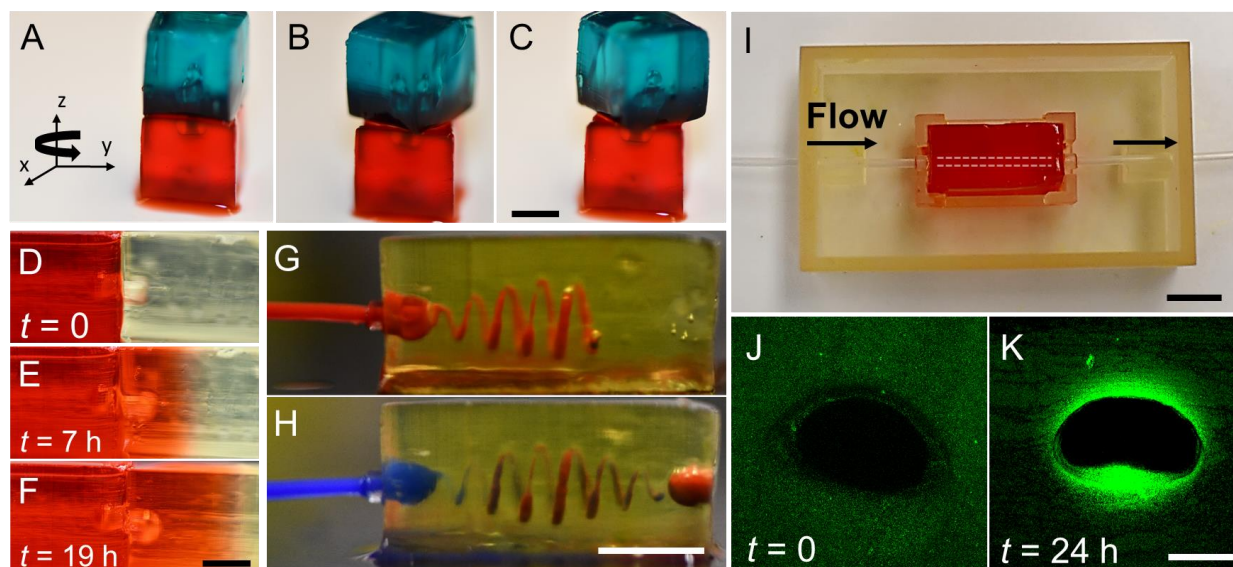415 10 mm, respectively.

416
417
418
419
420
421
422
423
424
425
426
427
428

Figure 6: *Pop-it connector advantages and potential applications*. (**A-C**) Connectors allow for free rotation around the long z-axis of the connector. The two gels are colored with red and blue food dye for clarity. (**D-F**) Two hydrogels held in contact by a two-sided connector allows diffusion of material from one gel into the other. Here, red food dye is used. (**G, H**) Connector reversibility allows multiple fluid streams to be sequentially introduced into the same hydrogel. (**I-K**) Long-term flow of media through a hydrogel containing bacteria enabled by connectors maintains cell growth and viability, (**I**) Hydrogel and tubing are assembled and held in a plastic 3D-printed holder. Fresh media is driven from left to right through the hydrogel. The gel is dyed red here for clarity. (**J, K**) Fluorescence confocal microscopy cross-sectional images of gel containing *Pseudomonas aeruginosa* (pMF230; constitutive GFP) before (**J**) and after (**K**) growth for 24 hours. Dark center hole is the cross-section of a semi-cylindrical channel ($D \approx 1.20$ mm). Scale bars correspond to: (H) 10 mm; (C), (F), and (H) 5 mm; and (K) 500 μm

460   1.   M. Mahinroosta, Z. J. Farsangi, A. Allahverdi and Z. Shakoori, *Mater Today Chem*, 2018, **8**, 42-55.
461   2.   H. J. Li, C. Tan and L. Li, *Mater Design*, 2018, **159**, 20-38.
462   3.   E. M. Ahmed, *J Adv Res*, 2015, **6**, 105-121.
463   4.   J. Saroia, Y. E. Wang, Q. H. Wei, K. Zhang, T. L. Lu and B. Zhang, *Bio-Des Manuf*, 2018, **1**, 265-279.
464   5.   J. M. Rosiak and F. Yoshii, *Nucl Instrum Meth B*, 1999, **151**, 56-64.
465   6.   J. M. Saul and D. F. Williams, *Pdl Handb Ser*, 2014, DOI: 10.1016/B978-0-323-22805-3.00012-8,
466   279-302.
467   7.   E. Calo and V. V. Khutoryanskiy, *Eur Polym J*, 2015, **65**, 252-267.
468   8.   Q. Y. Chai, Y. Jiao and X. J. Yu, *Gels-Basel*, 2017, **3**.
469   9.   B. Sidar, B. R. Jenkins, S. Huang, J. R. Spence, S. T. Walk and J. N. Wilking, *Lab Chip*, 2019, **19**, 3552-
470   3562.
471   10. B. H. Chueh, Y. Zheng, Y. S. Torisawa, A. Y. Hsiao, C. X. Ge, S. Hsiong, N. Huebsch, R. Franceschi, D.
472   J. Mooney and S. Takayama, *Biomed Microdevices*, 2010, **12**, 145-151.
473   11. A. D. Benjamin, R. Abbasi, M. Owens, R. J. Olsen, D. J. Walsh, T. B. LeFevre and J. N. Wilking,
474   *Biomed Phys Eng Expr*, 2019, **5**.
475   12. B. Grigoryan, S. J. Paulsen, D. C. Corbett, D. W. Sazer, C. L. Fortin, A. J. Zaita, P. T. Greenfield, N. J.
476   Calafat, J. P. Gounley, A. H. Ta, F. Johansson, A. Randles, J. E. Rosenkrantz, J. D. Louis-Rosenberg,
477   P. A. Galie, K. R. Stevens and J. S. Miller, *Science*, 2019, **364**, 458-+.
478   13. C. B. Goy, R. E. Chaile and R. E. Madrid, *React Funct Polym*, 2019, **145**.
479   14. Y. F. Zhou, *J Biomed Sci*, 2017, **24**.
480   15. H. J. Koo and O. D. Velev, *Biomicrofluidics*, 2017, **11**.
481   16. C. G. Xia and N. X. Fang, *Biomed Microdevices*, 2009, **11**, 1309-1315.
482   17. B. Dhariwala, E. Hunt and T. Boland, *Tissue Eng*, 2004, **10**, 1316-1322.
483   18. C. D. Spicer, *Polym Chem-Uk*, 2020, **11**, 184-219.
484   19. M. Schaffner, P. A. Ruhs, F. Coulter, S. Kilcher and A. R. Studart, *Sci Adv*, 2017, **3**.
485   20. M. Ogawa, K. Higashi and N. Miki, *2015 Transducers - 2015 18th International Conference on Solid-*
486   *State Sensors, Actuators and Microsystems (Transducers)*, 2015, 1692-1694.
487   21. L. E. Bertassoni, M. Cecconi, V. Manoharan, M. Nikkhah, J. Hjortnaes, A. L. Cristino, G. Barabaschi,
488   D. Demarchi, M. R. Dokmeci, Y. Z. Yang and A. Khademhosseini, *Lab Chip*, 2014, **14**, 2202-2211.
489   22. R. Sooppan, S. J. Paulsen, J. Han, A. H. Ta, P. Dinh, A. C. Gaffey, C. Venkataraman, A. Trubelja, G.
490   Hung, J. S. Miller and P. Atluri, *Tissue Eng Part C-Me*, 2016, **22**, 1-7.
491   23. I. S. Kinstlinger and J. S. Miller, *Lab Chip*, 2016, **16**, 2025-2043.
492   24. J. S. Miller, K. R. Stevens, M. T. Yang, B. M. Baker, D. H. T. Nguyen, D. M. Cohen, E. Toro, A. A.
493   Chen, P. A. Galie, X. Yu, R. Chaturvedi, S. N. Bhatia and C. S. Chen, *Nat Mater*, 2012, **11**, 768-774.
494   25. J. Nie, J. Z. Fu and Y. He, *Small*, 2020, **16**.
495   26. A. P. Wong, R. Perez-Castillejos, J. C. Love and G. M. Whitesides, *Biomaterials*, 2008, **29**, 1853-
496   1861.
497   27. A. M. Christensen, D. A. Chang-Yen and B. K. Gale, *J Micromech Microeng*, 2005, **15**, 928-934.
498   28. W. J. Chang, D. Akin, M. Sedlak, M. R. Ladisch and R. Bashir, *Biomed Microdevices*, 2003, **5**, 281-
499   290.
500   29. S. L. Faley, B. B. Baer, T. S. H. Larsen and L. M. Bellan, *Biomicrofluidics*, 2015, **9**.
501   30. R. Q. Hu, F. Li, J. Q. Lv, Y. He, D. T. Lu, T. Yamada and N. Ono, *Biomed Microdevices*, 2015, **17**.
502   31. J. N. Patel, B. Kaminska, B. L. Gray and B. D. Gates, *J Micromech Microeng*, 2008, **18**.
503   32. J. R. Ravetz, *Isis*, 1962, **53**, 263-266.
504   33. B. Yanez-Soto, S. J. Liliensiek, C. J. Murphy and P. F. Nealey, *J Biomed Mater Res A*, 2013, **101**,
505   1184-1194.
506   34. R. S. Seymour and A. J. Blaylock, *Physiol Biochem Zool*, 2000, **73**, 389-405.
507   35. K. C. Bhargava, B. Thompson and N. Malmstadt, *P Natl Acad Sci USA*, 2014, **111**, 15013-15018.

508   36.   P. Loskill, S. G. Marcus, A. Mathur, W. M. Reese and K. E. Healy, *Plos One*, 2015, **10**.
509   37.   L. J. Y. Ong, T. Ching, L. H. Chong, S. Arora, H. Li, M. Hashimoto, R. DasGupta, P. K. Yuen and Y. C.
510   Toh, *Lab Chip*, 2019, **19**, 2178-2191.
511   38.   S. Miserendino and Y. C. Tai, *Sensor Actuat a-Phys*, 2008, **143**, 7-13.
512   39.   A. W. Justin, R. A. Brooks and A. E. Markaki, *J R Soc Interface*, 2016, **13**.
513   40.   A. P. Golden and J. Tien, *Lab Chip*, 2007, **7**, 720-725.
514   41.   J. Nie, Q. Gao, Y. D. Wang, J. H. Zeng, H. M. Zhao, Y. Sun, J. Shen, H. Ramezani, Z. L. Fu, Z. J. Liu, M.
515   X. Xiang, J. Z. Fu, P. Zhao, W. Chen and Y. He, *Small*, 2018, **14**.
516   42.   C. N. LaFratta and L. J. Li, *Micro Nano Technol*, 2016, DOI: 10.1016/B978-0-323-35321-2.00011-X,
517   221-241.
518   43.   C. N. LaFratta, T. Baldacchini, R. A. Farrer, J. T. Fourkas, M. C. Teich, B. E. A. Saleh and M. J.
519   Naughton, *J Phys Chem B*, 2004, **108**, 11256-11258.
520   44.   C. D. Markert, X. Y. Guo, A. Skardal, Z. Wang, S. Bharadwaj, Y. Y. Zhang, K. Bonin and M. Guthold,
521   *J Mech Behav Biomed*, 2013, **27**, 115-127.
522   45.   B. D. Fairbanks, M. P. Schwartz, C. N. Bowman and K. S. Anseth, *Biomaterials*, 2009, **30**, 6702-
523   6707.
524   46.   F. Della Sala, M. Biondi, D. Guarnieri, A. Borzacchiello, L. Ambrosio and L. Mayol, *J Mech Behav*
525   *Biomed*, 2020, **110**.
526   47.   C. C. Xu, G. H. Dai and Y. Hong, *Acta Biomater*, 2019, **95**, 50-59.
527   48.   M. Ahearne, Y. Yang, A. J. El Haj, K. Y. Then and K. K. Liu, *J R Soc Interface*, 2005, **2**, 455-463.
528   49.   M. Y. Sun, X. T. Sun, Z. Y. Wang, S. Y. Guo, G. J. Yu and H. Z. Yang, *Polymers-Basel*, 2018, **10**.
529   50.   J. A. Stammen, S. Williams, D. N. Ku and R. E. Guldberg, *Biomaterials*, 2001, **22**, 799-806.
530   51.   R. Raman, B. Bhaduri, M. Mir, A. Shkumatov, M. K. Lee, G. Popescu, H. Kong and R. Bashir, *Adv*
531   *Healthc Mater*, 2016, **5**, 610-619.
532   52.   P. F. Jacobs, *Rapid Prototyping & Manufacturing: Fundamentals of Stereolithography*, 1992.
533